

Optical Engineering

OpticalEngineering.SPIEDigitalLibrary.org

External cavity cascade diode lasers tunable from 3.05 to 3.25 μm

Meng Wang
Takashi Hosoda
Leon Shterengas
Gela Kipshidze
Ming Lu
Aaron Stein
Gregory Belenky

SPIE.

Meng Wang, Takashi Hosoda, Leon Shterengas, Gela Kipshidze, Ming Lu, Aaron Stein, Gregory Belenky, "External cavity cascade diode lasers tunable from 3.05 to 3.25 μm ," *Opt. Eng.* **57**(1), 011012 (2017), doi: 10.1117/1.OE.57.1.011012.

External cavity cascade diode lasers tunable from 3.05 to 3.25 μm

Meng Wang,^a Takashi Hosoda,^a Leon Shterengas,^{a,*} Gela Kipshidze,^a Ming Lu,^b Aaron Stein,^b and Gregory Belenky^a

^aState University of New York at Stony Brook, Department of Electrical and Computer Engineering, Stony Brook, New York, United States

^bBrookhaven National Laboratory, Center for Functional Nanomaterials, Upton, New York, United States

Abstract. The external cavity tunable mid-infrared emitters based on Littrow configuration and utilizing three stages type-I quantum well cascade diode laser gain elements were designed and fabricated. The free-standing coated 7.5- μm -wide ridge waveguide lasers generated more than 30 mW of continuous wave power near 3.25 μm at 20°C when mounted epi-side-up on copper blocks. The external cavity lasers (ECLs) utilized 2-mm-long gain chips with straight ridge design and anti-/neutral-reflection coated facets. The ECLs demonstrated narrow spectrum tunable operation with several milliwatts of output power in spectral region from 3.05 to 3.25 μm corresponding to ~ 25 meV of tuning range. © 2017 Society of Photo-Optical Instrumentation Engineers (SPIE) [DOI: 10.1117/1.OE.57.1.011012]

Keywords: mid-infrared; GaSb; quantum cascade; external cavity laser; tunable laser.

Paper 170819SS received May 30, 2017; accepted for publication Aug. 24, 2017; published online Sep. 14, 2017.

1 Introduction

Compact and efficient spectroscopic sensors based on tunable narrow spectrum semiconductor lasers are in demand for industrial monitoring, medical diagnostics, home security, etc. The devices operating in the methane absorption band near 3.2 μm and utilizing wavelength specific distributed or external feedback elements have been reported, see for instance.^{1–4} Distributed feedback lasers are compact and robust but offer rather limited single mode tuning range (about several nm near 3 μm ⁵). External cavity lasers (ECLs) can demonstrate order of magnitude wider tuning range.^{6,7} Namely, for spectral region near 3.2 μm , about 60 nm of tuning range was reported for diode based,² about 85 nm for quantum cascade based,⁶ and about 110 nm for interband cascade based ECLs.⁴ Further extension of the tuning range requires broadening of the gain spectral bandwidth. Often the gain broadening implies reduction of the peak differential gain and, thus, increase of the threshold carrier concentration and threshold current. Excessive threshold current limits the tuning range indirectly by restricting the range of the operating temperatures compatible with continuous wave (CW) regime. Increase of the number of active quantum wells (QWs) can balance the effect of the gain broadening on the threshold current. However, carrier transport constraints often restrict the number of QWs that can be efficiently pumped in diode laser heterostructures. Cascade pumping scheme solves the carrier transport issues and enables efficient interband laser operation with large number of active QWs.⁸ Moreover, in cascade laser heterostructures with slightly different QWs in each cascade, the gain can be shaped to enhance the ECL tuning range. The number of stages required for an efficient operation for a given gain bandwidth depends on optical transition matrix element. The maximum values of interband transition matrix elements can be achieved in type-I QWs. The cascade diode lasers

utilizing type-I QWs and operating in spectral region near and above 3 μm were recently developed.⁹ In this work, we report on design and fabrication of the tunable ECLs based on three-stage cascade laser heterostructure and operating in methane absorption band near 3.2 μm . The lasers demonstrated more than 200 nm tuning range from 3.05 to 3.25 μm with several mW of CW output power at 20°C. The lasers were mounted epi-side up and used no electroplated thick gold to assist heat removal. The active QWs in each stage were not intentionally modified to yield broadened gain. The effect of the variation of the QW parameters in each cascade on ECL performance parameters and, specifically, tuning range will be subject of the separate studies.

2 Heterostructure Design and Device Fabrication

The laser heterostructure was grown on tellurium-doped GaSb substrates by solid source molecular beam epitaxy. Figure 1(a) shows the calculated heterostructure band diagram under the flat band condition. Optical gain was generated in three ~ 13 -nm-thick $\sim 1.5\%$ compressively strained GaInAsSb QWs with indium composition near 55%. The lasers utilized AlGaAsSb ~ 2 - μm -thick cladding layers containing $\sim 80\%$ of aluminum. Waveguide core was formed by ~ 300 -nm-thick GaSb layer between n-clad and the first QW, and ~ 350 nm of AlGaInAsSb (with $\sim 30\%$ of aluminum and indium contents) between the last QW and p-cladding.

The InAs/AlSb superlattice (SL) insert between GaSb and the first QW was added to confine holes in the first QW. The compositionally graded AlGaAsSb layers and chirped InAs/AlSb SL layers realized series connection of the three active QWs, i.e., cascade pumping scheme, see Ref. 10 for details. The wafer was processed into the ridge waveguide lasers. The ridges were etched using chlorine-based inductively coupled plasma (ICP) reactive ion etching (RIE) technique using the following parameters: $\text{BCl}_3/\text{Cl}_2/\text{Ar}$ —20/5/20 sccm, pressure ~ 3 mT, RIE power

*Address all correspondence to: Leon Shterengas, E-mail: leon.shterengas@stonybrook.edu

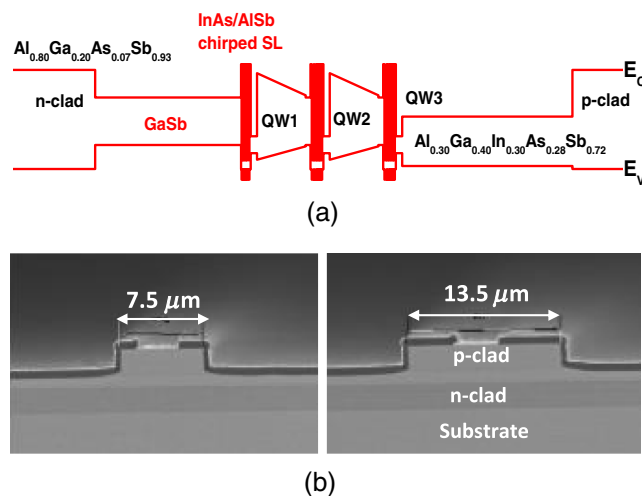


Fig. 1 (a) Schematic of band diagrams of laser heterostructure and (b) SEM images of the as-cleaved facet of ~ 7.5 - and ~ 13.5 - μm -wide ridge waveguide lasers.

200 W, and ICP power 300 W. The semiconductor etching rate was about 430 nm/min. The Si_3N_4 hard mask of initial thickness of ~ 600 nm was used (the mask etching rate was ~ 120 nm/min). The etching was stopped just below the interface between p-cladding and AlGaInAsSb layer so the active QWs were not etched through. We fabricated devices with ridge width varied from ~ 7.5 to ~ 13.5 μm . The p-contact metallization contained Ti/Pt/Au layer and Ti/Au overlay with ~ 200 nm of Au. Figure 1(b) shows scanning electron microscope images of the as-cleaved laser facets for the narrowest (left) and the widest (right) ridge waveguide lasers fabricated. After etching, the remnants of the hard mask were removed and ~ 600 -nm-thick Si_3N_4 layer was deposited. The laser wafer was lapped and polished down to ~ 150 μm . The Ni/Au/Ge/Ni/Au n-side contact was e-beam deposited, annealed in 5% hydrogen forming gas atmosphere, and covered by Ti/Pt/Au overlay. Uncoated 1-mm-long and coated 2-mm-long lasers were tested in standalone and external cavity configurations.

3 Operation of the Standalone Ridge Lasers

Figure 2 plots the light-current-voltage characteristic of the 1-mm-long uncoated lasers with variable ridge width characterized in short pulse low duty cycle regime (100 kHz/200 ns) at room temperature (20°C). The laser threshold increases from ~ 65 to ~ 75 mA when the ridge waveguide width changes from ~ 7.5 to 13.5 μm . The two-facet device external efficiency increases with the ridge width from $\sim 60\%$ to $\sim 70\%$ (the two-facet external efficiency of the benchmark 100- μm -wide deep etched ridge waveguide lasers was $\sim 95\%$ per three cascades). The lateral far-field patterns for 7.5- and 13.5- μm -wide ridges measured at the currents just above the threshold and at about three thresholds are shown in the insets in Fig. 2. The 13.5- μm -wide ridges demonstrate clear tendency to multiple spatial mode behavior showing double peak far-field patterns at increased currents. The 7.5- μm -wide ridges generate beams with the single lobe far-field patterns at all currents, though the beam divergence somewhat increased with the current. The near-field patterns were imaged using InSb-based

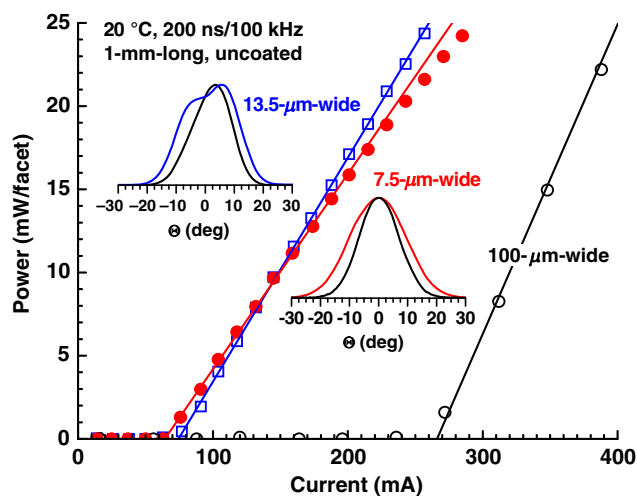


Fig. 2 Light-current characteristics of the 7.5-, 13.5-, and 100- μm -wide ridge waveguide 1-mm-long uncoated lasers measured in low duty cycle pulse regime (100 kHz/200 ns) at 20°C. Insets plot the lateral far-field patterns measured for 7.5- and 13.5- μm -wide ridge lasers at two currents: above but near thresholds (narrower patterns) and at about three thresholds (wider pattern).

infrared camera. Virtually no change in the near field was observed with the current increase. The stability of single lobe near-field patterns was interpreted as an indication of the stable single spatial mode device operation for all currents above threshold. Thus we selected 7.5- μm -wide ridges for external cavity experiments. The modal gain spectra measured at several currents under threshold for 7.5- μm -wide ridge lasers (Fig. 3) can be used to estimate the laser internal loss to be 9 to 10 cm^{-1} . The 100- μm -wide deep ridge multi-mode lasers demonstrated only 2 to 3 cm^{-1} lower values of internal loss.⁹

The internal loss increase in narrow ridge lasers compared to wide ridge devices cannot fully explain the observed difference in their slope efficiencies (Fig. 2). The nominal

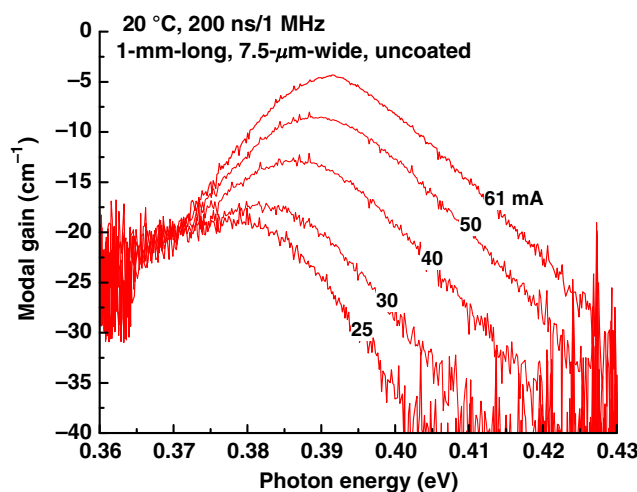


Fig. 3 Modal gain spectra of the 7.5- μm -wide ridge waveguide 1-mm-long uncoated laser measured by Hakki-Paoli method¹¹ at several under threshold currents in pulse regime (200 ns/1 MHz) at 20°C. The long wavelength part of all gain spectra tends to saturate to the modal gain value equal to the total cavity loss.

threshold current density of the 7.5- μm -wide lasers would be above 850 A/cm² if the physical ridge width were used as a current aperture. This would comprise more than threefold increase over ~ 270 A/cm² observed for 100- μm -wide emitters. Lateral current spreading in the narrow ridge lasers can contribute to the reduction of the device slope efficiency and explain excessive nominal values of the threshold current densities of the narrow ridge lasers compared to 100- μm -wide benchmark devices (Fig. 2). Thus one can speculate that the relatively shallow etching (Fig. 1) does not confine current under the ridge. The etching through the active region would be necessary to achieve strong current confinement. However, surface recombination at the etched sidewalls might diminish the associated benefits.⁹

Figure 4(a) plots the light-current-voltage characteristics of the 2-mm-long coated lasers with ridge width of 7.5 μm . Two types of devices were tested in CW regime at 20°C in epi-side-up configuration: anti-/high-reflection (AR/HR) and ultralow anti-/neutral-reflection (AAR/NR) coated lasers. The latter one was designed for external cavity operation

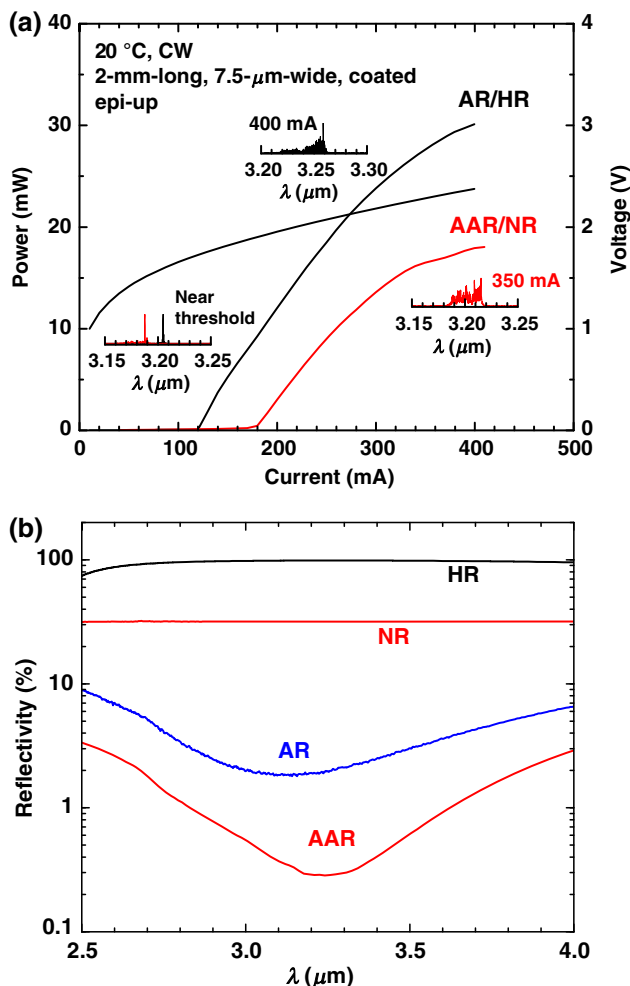


Fig. 4 (a) Light-current-voltage characteristics of the free running 7.5- μm -wide ridge waveguide, 2-mm-long, AR/HR, and AAR/NR coated devices mounted epi-side-up and characterized in CW regime at 20°C. Insets show the laser spectra near threshold and at the maximum output power levels. (b) The measured reflectivity spectra of the reference silicon samples coated together with the corresponding laser facets.

with AAR coated mirror to face the external grating feedback element. Figure 4(b) plots the reflectivity spectra measured for the control reference silicon samples coated together with the corresponding laser facets. The HR coating comprised of two-period Al₂O₃/Si Bragg reflector demonstrated reflectivity $\sim 98\%$ near 3.2 μm . The NR coating was made of thin layer of Al₂O₃ and showed reflectivity of about 32%. Single quarter wavelength Al₂O₃ layer was used to fabricate AR coating with reflectivity $\sim 2\%$, while triple layer Al₂O₃/Si/Al₂O₃ AAR coating demonstrated reflectivity $\sim 0.3\%$. The laser effective modal index of about 3.45 near 3.2 μm can be estimated. The refractive index of silicon is about 3.43. Thus, one can expect relatively close correspondence between reflectivity of the coated laser facets and measured values for the reference samples. The estimated mirror loss for AR/HR and AAR/NR devices was about 10 and 17 cm⁻¹, respectively. Since the mirror loss of the uncoated 1-mm-long lasers are 11 to 12 cm⁻¹, one can expect the gain spectra at the threshold of the 2-mm-long AR/HR coated lasers to be similar to the threshold gain spectra of 1-mm-long uncoated laser (61 mA curve in Fig. 3). The AAR/NR devices require stronger pumping to overcome ~ 7 cm⁻¹ higher total loss. This explains larger threshold and blue shifted spectra of the AAR/NR lasers compared to AR/HR ones. Both types of devices generated in excess of 15 mW of CW power at 20°C when mounted epi-side-up. The power shown in Fig. 4 for AAR/NR laser was collected from AAR coated facet.

4 External Cavity Laser Operation

The 2-mm-long, 7.5- μm -wide ridge waveguide devices coated AAR/NR were tested as a gain element in the Littrow configuration. The ECL output was collected from NR coated mirror of the epi-side-up mounted laser chip. The light from AAR coated mirror was collimated by aspheric lens (NA ~ 0.85 , focal length: 1.875 mm) and directed to blazed grating (450 groves/mm, 1.6 nm/mrad) that was positioned about 20 cm away from the lens. Figure 5(a) plots the spectra of the ECL near the threshold for various grating angles. The laser line intensities are scaled to match the corresponding threshold currents. The spectra of the free-running AAR/NR and AR/HR lasers are also shown with their baselines shifted to the corresponding laser thresholds. The lowest thresholds of about 120 mA were observed for ECL with minimal detuning of the grating feedback wavelength from the gain peak. Increase of the detuning led to increase of the ECL threshold until threshold of the stand-alone AAR/NR was reached and laser started operating in multimode regime near the wavelength corresponding to the gain peak. The threshold current of the ECL laser with minimal detuning was very close to the threshold of the free running AR/HR laser. Based on the difference of the mirror loss between AR/HR and AAR/NR coated free-running devices (difference is ~ 7 cm⁻¹), one can estimate the amount of feedback received from the grating to be equivalent to 6% to 7% of the mirror reflectivity. The difference in modal gain at the peak and at 380 and 405 meV that can be estimated from Fig. 3 is indeed ~ 7 cm⁻¹ for the near threshold spectra of AR/HR lasers. Though stronger pumping is needed for AAR/NR devices it is expected that the difference between peak and 380/405 meV gain values would remain close to that value. Asymmetry of the gain

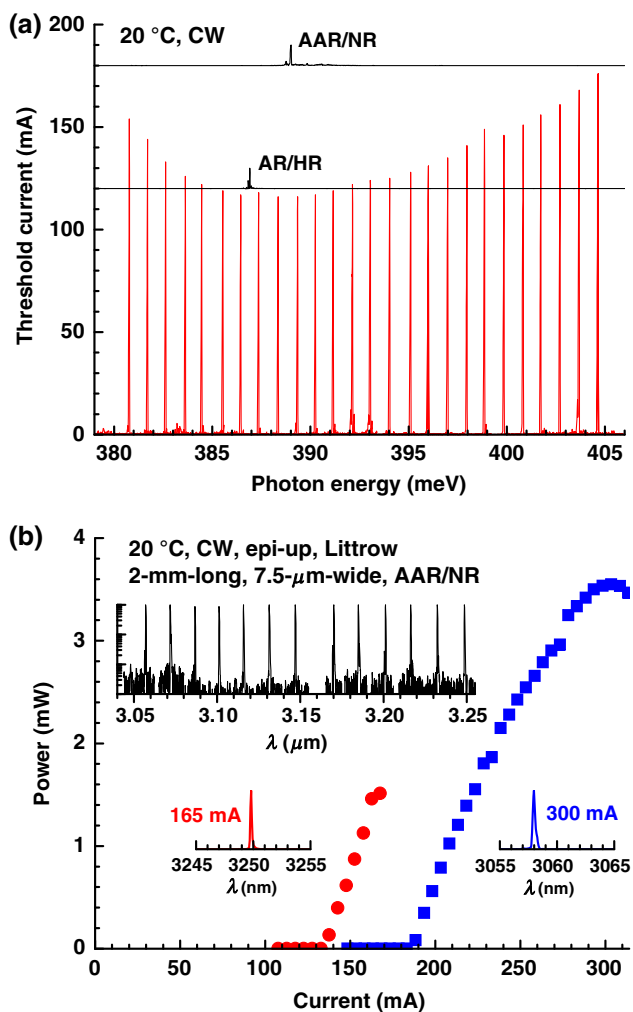


Fig. 5 Near threshold emission spectra of the ECL normalized to the corresponding value of the laser threshold. Spectra of the free running AAR/NR and AR/HR coated devices are shown with their baseline shifted to match their threshold currents. (b) Light-current characteristics of the ECL tuned to 3.26 and 3.06 μm . Corresponding laser spectra are shown next to the light-current curves. The top inset shows the normalized ECL spectra corresponding to maximum output power levels at different grating angles.

spectra (Fig. 3) explains the twice wider tuning range in the short wavelength direction. The differential gain on the longer wavelength side of the gain spectra is lower, leading to rapid increase of the ECL threshold current with detuning in that direction. Overall tuning range was approaching 25 meV. Figure 5(b) shows light-current characteristics measured for ECL narrow spectrum operation roughly corresponding to the boundaries of the tuning range. Inset (top) to the Fig. 5(b) shows the normalized ECL spectra corresponding to the maximum single mode output power levels. The single frequency operation (measurement resolution 0.125 cm^{-1}) with side mode suppression ratio better than $\sim 25\text{ dB}$ was obtained. It should be noted that measurement noise level was limiting the experimental estimate for side mode suppression ratio. The noise originated from the necessity to strongly attenuate the input to Fourier transform spectrometer to avoid artificial spectral features.

The CW power of the laser emitting near 3.06 μm was limited by thermal roll-over while the power near 3.25 μm

was limited by jump to multimode operation at the wavelength corresponding to the gain peak. The ECL generated more than 2 mW of single frequency tunable CW power in the spectral range of about 200 nm centered near 3.15 μm . It should be noted that when the gain chip was run in short pulse regime (200 ns/1 MHz) and grating was positioned closer to AAR coated facet, the average ECL output spectrum became multimode. The possible explanation can involve μm -scale mechanical displacements caused by minute temperature oscillations. The mrad-scale misalignment could be caused, for instance, by lateral shifts of the laser die by a couple of μm with respect to collimating lens. For a given grating angular dispersion (1.6 nm/mrad), the average nm-scale spectral range will be coupled back to the laser cavity. These considerations explain relatively long external cavity length used for ECL demonstration. Namely, the 7.5- μm -wide ridge would accept the light within $\sim 2\text{ mrad}$ range leading to efficient feedback in the spectral region of $\sim 3\text{ nm}$ if the grating is located too close to the collimating lens.

5 Summary

Straight ridge waveguide anti-reflection coated GaSb-based type-I QW cascade diode laser gain elements were used in Littrow external cavity configuration. The tuning range of about 25 meV corresponding to the gain width at about 7 cm^{-1} level below the peak was demonstrated. The devices generated milliwatts of single frequency power tunable from 3.05- to 3.25- μm spectral region. The free running AR/HR coated lasers generated in excess of 30 mW of CW output power at 20°C near 3.25 μm . Both free running lasers and ECL gain elements were mounted epi-side-up on gold plated copper blocks. The demonstrated tuning range is one of the largest reported in this spectral region and can be further extended by about 10 meV when cascade diode laser heterostructures with variable QW parameters are utilized as gain elements.¹²

Acknowledgments

This work was supported by the National Science Foundation, Grant ECCS-1408126US, and Army Research Office, Grant W911NF1110109 and in part by the U.S. Department of Energy, Office of Basic Energy Sciences, through the Center for Functional Nanomaterials, Brookhaven National Laboratory, under Contract DE-SC0012704.

References

1. R. Liang et al., "Distributed feedback 3.27 μm diode lasers with continuous-wave output power above 15 mW at room temperature," *Electron. Lett.* **50**(19), 1378–1380 (2014).
2. J. A. Gupta et al., "High-resolution methane spectroscopy using InGaAsSb/AlInGaAsSb laterally-coupled index-grating distributed feedback laser diode at 3.23 μm ," *Electron. Lett.* **48**(7), 396 (2012).
3. S. Forouhar et al., "Reliable mid-infrared laterally-coupled distributed-feedback interband cascade lasers," *Appl. Phys. Lett.* **105**(5), 051110 (2014).
4. D. Caffey et al., "Performance characteristics of a continuous-wave compact widely tunable external cavity interband cascade lasers," *Opt. Express* **18**(15), 15691–15696 (2010).
5. T. Hosoda et al., "Laterally coupled distributed feedback cascade diode lasers emitting near 2.9 μm ," *Electron. Lett.* **52**(10), 857–859 (2016).
6. T. Kruczek et al., "InAs/AlSb widely tunable external cavity quantum cascade laser around 3.2 μm ," *Appl. Phys. Lett.* **102**(1), 011124 (2013).

7. K. Vizbaras et al., "High power continuous-wave GaSb-based superluminescent diodes as gain chips for widely tunable laser spectroscopy in the 1.95 – 2.45 μm wavelength range," *Appl. Phys. Lett.* **107**(1), 011103 (2015).
8. I. Vurgaftman et al., "Interband cascade lasers with low threshold powers and high output powers," *J. Sel. Top. Quant. Electron.* **19**(4), 1200210 (2013).
9. L. Shterengas et al., "Cascade pumping of 1.9 – 3.3 μm type-I quantum well GaSb-based diode lasers," *J. Sel. Top. Quant. Electron.* **23**(6), 1500708 (2017).
10. L. Shterengas et al., "Cascade type-I quantum well diode lasers emitting 960 mW near 3 μm ," *Appl. Phys. Lett.* **105**(16), 161112 (2014).
11. B. W. Hakki and T. L. Paoli, "Gain spectra in GaAs double-heterostructure injection lasers," *J. Appl. Phys.* **46**(3), 1299–1306 (1975).
12. L. Shterengas et al., "Cascade type-I quantum well GaSb-based diode lasers," *Photonics* **3**(2), 27 (2016).

Biographies for the authors are not available.